nature research

https://doi.org/10.1038/s41557-020-00575-0

Supplementary information

Predator–prey interactions between droplets driven by non-reciprocal oil exchange

In the format provided by the authors and unedited

Supplementary Materials for

Predator-Prey Interactions between Droplets Driven by Nonreciprocal Oil Exchange

Caleb H. Meredith[1†], Pepijn G. Moerman[2,3†], Jan Groenewold[2,4], Yu-Jen Chiu[1], Willem K. Kegel[2], Alfons van Blaaderen[3], Lauren D. Zarzar[1,5,6*]

1. Department of Materials Science and Engineering, The Pennsylvania State University, PA 16802, USA
2. Van't Hoff Laboratory for Physical & Colloid Chemistry, Debye Institute for Nanomaterials Science, Utrecht University, The Netherlands
3. Soft Condensed Matter, Debye Institute for Nanomaterials Science, Utrecht University, The Netherlands
4. Guangdong Provincial Key Laboratory of Optical Information Materials and Technology & Institute of Electronic Paper Displays, South China Academy of Advanced Optoelectronics, South China Normal University, Guangzhou 510006, P. R. China.
5. Department of Chemistry, The Pennsylvania State University, PA 16802, USA
6. Materials Research Institute, The Pennsylvania State University, PA 16802, USA

† These authors contributed equally to this work

Correspondence to: ldz4@psu.edu

Supplementary Discussion

Quantification of interaction energy and displacement energy for two-body droplet chasing. To measure the energies associated with the predator-prey interaction of a droplet pair, we measured both the change in the droplet separation distance with time, $\delta r/\delta t$, and the velocity of the midpoint between the droplets, $v_{midpoint}$, as a function of the inter-particle distance, r. At droplet separations larger than 130 μm, the droplet velocities due to solute-mediated interactions were small compared to the drift velocity, so we only measured interactions for droplets closer than 130 μm and considered droplets at larger separations to be isolated. To minimize contributions from drift in the calculations, we measured $v_{midpoint}$ and $\delta r/\delta t$ for isolated droplets (which do move from drift) and subtracted those values from velocity measurements for interacting droplets at small separation distances so that we isolate the component of the droplet speed that is due to chemotactic interactions. We averaged $v_{midpoint}$ and $\delta r/\delta t$ as a function of drop separation distance attained from 3 to 5 separate experiments using bins of 1 μm in inter-droplet separation.

At low Reynolds numbers, the energy associated with the interaction between two droplets $E_{interaction}$ equals the area under the curve $\delta r/\delta t$ versus r times the drag constant C_D, where we took the drag constant to be equal to the Stokes' drag multiplied by a dimensionless factor *C* that corrects for flow inside the droplet and proximity of the droplet substrate. Note that, because the correction for proximity to the substrate strongly depends on the distance between

the droplet and the substrate, we cannot easily estimate the magnitude of *C* but instead assume that it is constant between experiments and just report interactions scaled by this dimensionless factor. We thus found $\frac{E_{interaction}}{C} = 6\pi\eta a \int_{r=2a}^{r=\infty} \delta r/_{\delta t}\, dr$, where $\eta = 0.89$ mPa s is the viscosity of the aqueous solution and a is the droplet radius. The sign of this interaction energy does not indicate whether energy was consumed or produced, but rather whether the interaction was repulsive (positive) or attractive (negative). The energy associated with the displacement of the midpoint of the chasing pair is $\frac{E_{displacment}}{C} = 6\pi\eta a \int_{r=2a}^{r=\infty} v_{midpoint} dr$. The sign of the displacement energy indicates the direction of the chase, where we arbitrarily defined a positive displacement energy to correspond to a chase in which the fluorinated oil is prey (as seen in **Figure 2**).

Quantification of interaction parameters for simulations. We compared experimentally observed cluster dynamics of bromooctane (BOct) droplets mixed with ethoxynonafluorobutane (EFB) or methoxynonafluorobutane (MFB) droplets with overdamped particle dynamics simulations of particles interacting through chemotactic forces. We used the form of the speed of droplet 1 due to chemotactic forces exerted by droplet 2: $\overrightarrow{v_{12}} = C_{12} \frac{\overrightarrow{r_{12}}}{|\overrightarrow{r_{12}}|^3}$ that was predicted by Soto and Golestanian(*21)*, where $\overrightarrow{r_{12}}$ is the center-to-center separation between drop 1 and 2 and C_{12} is an interaction constant with units μm^3/s. Soto and Golestanian assume that the Péclet number of the particles is small (i.e. fast diffusive transport of solute compared to advective transport due to the motion of the particle) so that the particles only interact *via* spherically symmetric concentration profiles with no hydrodynamic disturbances. Then $C_{12} = M_1 A_2$, where the mobility, M, is a measure for the speed a particle acquires in a given solute gradient and the activity, A, is a measure for the rate of solute production or consumption on the particle's surface.

In our experiments, the Péclet number $Pe = \frac{v\,a}{D} \sim 1$ to 10, estimated for droplets with a radius $a \approx 35$ μm, moving at $v \approx 20$ μm/s and assuming that the relevant solute are oil-filled micelles with diffusion constant $D \sim 10^{-11} m^2/s$. For high Péclet numbers, hydrodynamic disturbances do quantitatively affect the solute-mediated interactions and C_{12} depends on the particle velocity; when the Péclet number exceeds a critical Péclet number of 4, the particles are predicted to self-propel due to these hydrodynamic deformations of the solute concentration profiles (*28*). Indeed, we found a subset of BOct droplets to self-propel, confirming that the Péclet number of our droplets is close to 4. Surprisingly, the subset of self-propelled droplets were below a typical size of approximately 40 μm in diameter, whereas the Péclet number is predicted to increase with size (for reaction-limited solute production) or be size independent (for diffusion limited solute production) but not decrease with size (*16*). We do not have an explanation for this observation.

Despite this high Péclet number where hydrodynamic effects will quantitatively impact solute-mediated interactions, we found that the speed of a droplet in the gradient of its neighbor still roughly scales with distance as $1/r^2$. This observation suggests that for droplet pairs under fixed conditions we can extract effective interaction parameters C_{12} to use in simulations to recapitulate the qualitative dynamics of droplet pairs, but those effective parameters cannot be interpreted as the product of a mobility and activity directly because they also contain hydrodynamic contributions.

To compare the multibody simulations directly with experiments, we set out to extract these effective interaction constants, C_{qp} and C_{pq} from observed two-body droplet interactions, where we introduce the convention that "p" indicates the predator (BOct) and "q" indicates the prey (EFB or MFB). C_{qp} determines the speed $\overrightarrow{v_{qp}}$ with which a prey droplet moves due to the chemotactic interaction with a predator, and C_{pq} similarly determines the predator speed $\overrightarrow{v_{pq}}$ due to the interaction with a prey droplet. To this end, we tracked droplet positions during two-droplet encounters between a predator and a prey and measured the component of the velocity of the prey that points away from the midpoint between the prey and predator: $v_{qp} = \frac{\overrightarrow{v_q}\cdot(\overrightarrow{r_q}-\overrightarrow{r_p})}{|\overrightarrow{r_q}-\overrightarrow{r_p}|}$, where $\overrightarrow{r_q}$ and $\overrightarrow{r_p}$ are the position of the prey and predator droplet respectively. The speed v_{qp} is positive if the prey moves away from the predator and negative if the prey moves toward the predator. **Supplementary Fig. 1** shows that a graph of v_{qp} versus the inverse squared droplet separation ${r_{qp}}^{-2}$ is approximately a straight line from which we extracted the interaction constant C_{qp} using the Matlab least squares fitting procedure. Similarly, we measured the interaction constant C_{pq} from a curve of the experimentally measured v_{pq} versus ${r_{qp}}^{-2}$.

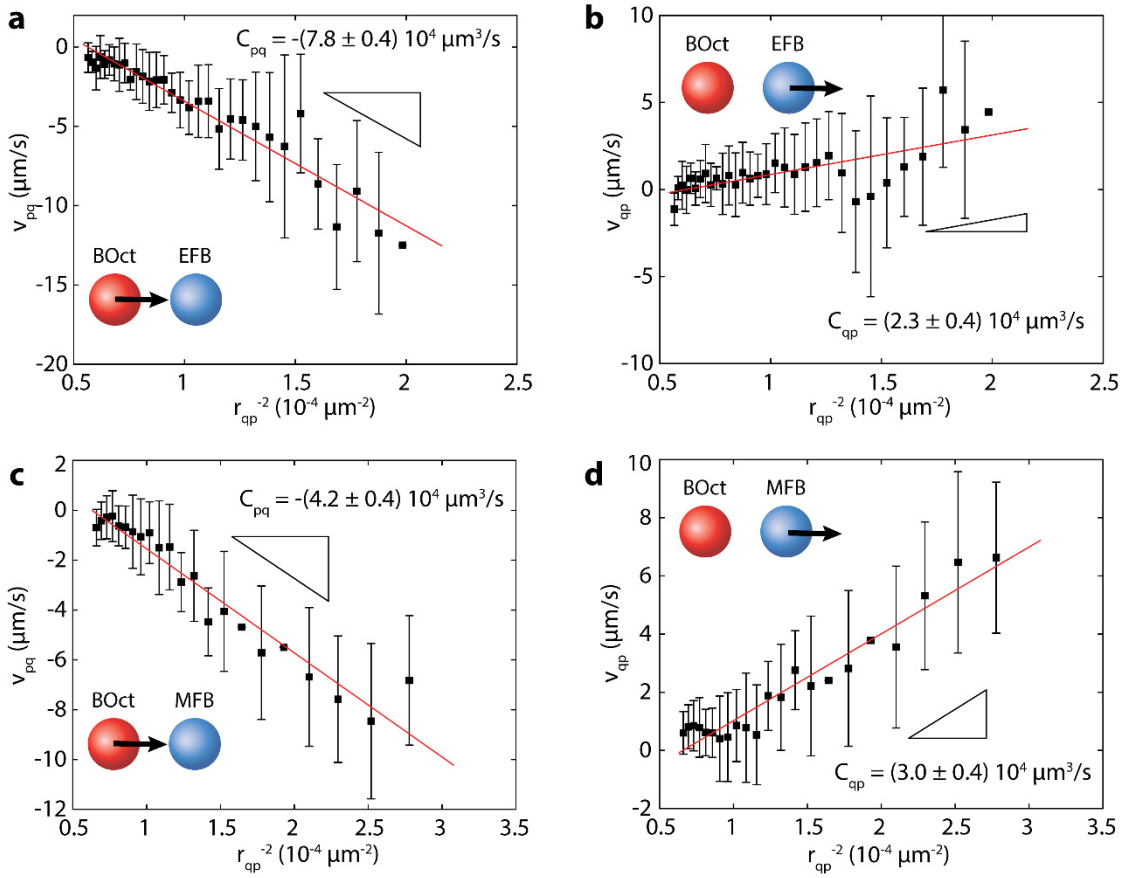

Supplementary Fig. 1. Measurements of the two-droplet interaction constants C_{qp} and C_{pq} for encounters between BOct drops and either EFB or MFB droplets. **a**, Approach speed of BOct droplets near EFB droplets. **b**, Escape speed of EFB droplets near BOct droplets. **c**, Approach speed of BOct droplets near MFB droplets. **d**, Escape speed of MFB droplets near BOct droplets. The data in each plot are measured from three separate two-droplet encounters.

The speed versus distance curves were binned with 1 μm bins. The data represent the average speed per bin and the error bar represents the standard deviation.

We did not observe interactions of sufficient strength between two prey drops to measure C_{qq}, which determines the speed of prey due to interactions with another prey, or between two predator droplets to measure C_{pp}, which determines the speed of a predator due to interaction with another predator. To find those two interaction parameters C_{qq} and C_{pp}, we measured the distance between two predator drops, r_{pp}, in a cluster of two predators and one prey as shown in **Supplementary Fig. 2.** This distance r_{pp} is set by a balance of the component of the speeds of the predators toward each other due to their interaction with the prey and the speeds of the predators away from each other due to mutual predator-predator repulsion:

$$\frac{C_{pp}}{{r_{pp}}^2} = \frac{C_{qp}\sin\left(\frac{1}{2}\theta\right)}{{r_{qp}}^2}. \qquad \text{Eq. S1}$$

Here θ is the angle the two predators and the prey make with each other, r_{pp} is the center-to-center distance between the predators, and r_{qp} is the center-to-center distance between the predator and prey, which at contact is given by the sum of predator and prey radii. The distances r_{qp} and r_{pp} were measured from the cluster geometry and C_{qp} was independently measured from two-body chasing interactions as just previously described, so that we can calculate C_{pp}. We realize that this is a rough estimate of C_{pp} because C_{qp} was measured from a speed vs. distance curve, where hydrodynamic effects play a role, whereas this measurement of C_{pp} is based on a static geometry as a consequence of balancing forces where hydrodynamic effects do not play a role. Finally, we find C_{qq} using the fact that the four interaction constants $C_{qq}, C_{qp}, C_{pq}$and C_{pp} are related through:

$$C_{qq} = \frac{C_{qp}C_{pq}}{C_{pp}}. \qquad \text{Eq. S2}$$

The relation in Equation S2 uses the fact that the interaction constant $C_{12} = \frac{\mu_1\alpha_2}{D}$ depends on the mobility of droplet 1, μ_1, which determines the speed of the droplet in a solute gradient due to the Marangoni effect and on the activity α_2, that represents the rate at which molecules are produced or consumed at the surface of droplet 2*(21)*. This activity divided by the diffusion constant of the solute, D, determines the solute gradient that causes droplet 1 to move. Using this definition we find that $\frac{C_{qp}C_{pq}}{C_{pp}} = \frac{\mu_q\alpha_p\mu_p\alpha_q D}{\mu_p\alpha_p D^2} = \frac{\mu_q\alpha_q}{D} = C_{qq}$. We list the interaction values we found for interactions between BOct and EFB or MFB droplets in **Supplementary Table 1**.

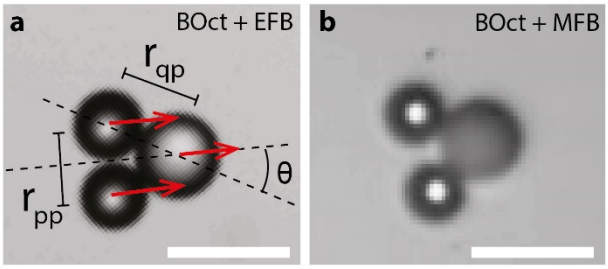

Supplementary Fig. 2. Spacing between predator droplets when two predators chase a single prey. a, Two BOct droplets chasing a single EFB droplet. The BOct droplets nearly touch. **b**, Two BOct droplets chasing an MFB droplet. The spacing between two BOct droplets is much larger than in a similar cluster with an EFB droplet. Scale bars are 100 μm.

Supplementary Table 1. **List of experimentally determined interaction parameter values obtained from two-body chasing encounters of BOct droplets with EFB or MFB droplets as well as the specific value of each parameter used in the simulations.** Results of the simulations with the given parameters are shown in **Figure 4**. The parameters used in the simulations were chosen from within the experimentally determined range to yield droplet dynamics that most closely matched the experiment.

	BOct and EFB		BOct and MFB	
	Experiment	Simulation	Experiment	Simulation
C_{pp} (10^4 μm^3/s)	-4.8 ± 1.6	-4.8	-4.8 ± 1.6	-4.9
C_{pq} (10^4 μm^3/s)	2.3 ± 0.4	2.3	2.9 ± 0.4	2.5
C_{qp} (10^4 μm^3/s)	-7.8 ± 0.4	-7.8	-4.2 ± 0.4	-3.8
C_{qq} (10^4 μm^3/s)	3.7 ± 0.4	3.7	3.2 ± 1.0	4.2

We initialized the simulations of multi-body droplet interactions by placing n_p predator and n_q prey drops on positions that match the positions in an experiment. Then, we calculated the speed $\overrightarrow{v_p}$ of each predator drop p and prey drop q, $\overrightarrow{v_q}$, by summing the contributions of each other droplet to the phoretic velocity as

$$\overrightarrow{v_p} = \sum_{i=1, i\neq p}^{n_p} C_{pp} \frac{\overrightarrow{r_{ip}}}{|\overrightarrow{r_{ip}}|^3} + \sum_{j=1}^{n_q} C_{pq} \frac{\overrightarrow{r_{jp}}}{|\overrightarrow{r_{jp}}|^3}, \qquad \text{Eq. S3}$$

$$\overrightarrow{v_q} = \sum_{i=1}^{n_p} C_{qp} \frac{\overrightarrow{r_{iq}}}{|\overrightarrow{r_{iq}}|^3} + \sum_{j=1, j\neq q}^{n_q} C_{qq} \frac{\overrightarrow{r_{jq}}}{|\overrightarrow{r_{jq}}|^3}, \qquad \text{Eq. S4}$$

Here i and j are indices that designate predator and prey drops respectively. The displacement in a time step dt is then given by $d\vec{r} = \vec{v}dt$. We chose the time step dt such that it was always smaller than the smallest drop radius divided by the largest possible speed for a given set of initial conditions. Typically, 10^{-2} s < dt < 10^{-3} s. We chose the number of time steps n based on the length of the experimentally observed interaction and n typically varied from $n = 10^3$ to $n=10^4$. We treated the droplets as hard spheres and resolve overlap using inelastic collisions.

Because we measured three of the four interaction constants directly, $C_{pp}, C_{qp,} C_{pq}$ and calculated the fourth constant C_{qq} from Equation S2**,** we can directly compare our simulations with the experiments. We tuned the parameters used in the simulations within the uncertainty range of the measured values to match the experimentally observed dynamics as closely as possible.

Trochoidal trajectories. Based strictly on the concept of chemotactic forces, we would expect that a predator droplet chasing after prey would always move in a straight line, assuming no other forces from neighboring droplets are introduced. Instead, we commonly observed trochoidal trajectories with a steady pitch for BOct chasing of either EFB or MFB, as shown in **Figure 4B**. Such trajectories were most often observed when the BOct droplets were small, under approximately 40 μm diameter. Based on the observation that BOct droplets become self-propelled and move at a significantly faster velocity when they shrink to a diameter below about 40 μm (**Extended Data Fig. 6**), we speculate that the reason for this trochoidal motion is that the BOct predator drop moves along the prey's surface during the chase due to its self-propulsion. This rearrangement of the predator on the surface of the prey causes the prey droplet to turn in response, because it always moved away linearly from the predator, leading to a redirect of the chase direction.

Extended Data Fig. 7 shows the absolute speed of a predator and prey droplet in a typical trochoidal chase. The predator drop indeed moved slightly faster than the prey; however, this phenomenon should cause the pair to swim in circles, not along trochoidal trajectories. We also observe that the speed of the chasing pair depends on its orientation (resulting in oscillations in speed over time) which causes the chasers to move along a trochoidal rather than a circular trajectory. We speculate that a possible cause of this orientation-dependent speed could be symmetry breaking due to the trail of oil-filled micelles left behind by the chasing pair. It has also been proposed that hydrodynamic effects could be responsible for symmetry breaking if swimmers are hydrodynamic pushers (*11*); the flow profile shown in **Extended Data Fig. 5** is consistent with a pusher geometry, making this explanation plausible as well.

Efficiency of chasing driven by oil exchange. We consider here the motion of a pair of droplets that exchange oil with one another through the aqueous Triton X-100 surfactant phase, where the two droplets consist of iodo-*n*-alkanes of differing *n*. The iodoalkanes are miscible in any ratio so that, when the droplets are in close proximity, there is iodoalkane transport from the droplet through the surfactant solution phase into the neighboring droplet and vice-versa. For droplets of different iodoalkanes, this oil exchange is asymmetric such that there is a net oil transport between droplets. The asymmetric oil transport drives chasing and propels the motion of the droplet pair with speeds of $20\ \mu m/s$ or more through coupling with the local droplet interfacial tensions and the Marangoni effect.

To estimate the efficiency of this propulsion mechanism, we assume that the mixing of the two oils is ideal and ignore contributions from the surface energy. The assumption that the mixing is ideal is reasonable because the two oils are miscible in any ratio and are chemically very similar. Any enthalpic effects that are ignored would most likely only decrease Gibbs free energy of mixing, rendering this estimate of the propulsion efficiency a lower boundary. For droplets of similar diameter, any contributions of the surface energy to the Gibbs free energy change of oil exchange would be small. To calculate the efficiency, we compare the Gibbs free energy of mixing with the displacement work of the pair of droplets. To simplify the calculation,

we consider specifically the input power (i.e. the Gibbs free energy of mixing per unit time) with the output power, which is related to the velocity of the droplets.

We make an order of magnitude estimate of the output power P_{out} from the velocity of the chasing droplet pair, assuming that the drag on these droplets is the Stokes' drag and ignoring modifications due to the proximity of the wall, nearby droplets, and the fact that the drops are fluid; thus, the force exerted on a droplet pair, F_{pair}, causing it to move with a velocity v_{pair} is $F_{pair} \approx 6\,\pi\,\eta\,a\,v_{pair}$, where $\eta = 0.89\ \mathrm{mPa \cdot s}$ is the viscosity of the aqueous surfactant solution and a is the radius of the droplets. The power consumption by the pair of droplets is then simply the force exerted on the droplets multiplied by the distance over which the force was applied and divided by the time it took to cross that distance, so we find

$$P_{out} \approx\ 6\,\pi\,\eta\,a\,{v_{pair}}^2 \qquad \text{Eq. S5}$$

For example, for droplets with a diameter of 70 μm that move at $20\ \mu\mathrm{m/s}$, the dissipated power is $P_{out} \approx 2.3 \times 10^{-16}\ \mathrm{J/s}$. This power required to move the pair of droplets comes from a change in the Gibbs free energy of mixing of the two oils, $\Delta_{mix}G = -T\Delta_{mix}S$, where we assume ideal mixing and ignore interfacial contributions. For a binary mixture, the entropy gain is $\Delta_{mix}S = -n\,R\,(x\ln(x) + (x-1)\ln(x-1))$, where n represents the amount of mixed oil in moles, $R = 8.314\,\frac{\mathrm{J}}{\mathrm{mol\,K}}$ is the ideal gas constant, and x is the mole fraction of one oil in the other after mixing. The maximum energy gain corresponds to mixing of equal molar amounts of oil in a 1:1 mixture, where $x = 0.5$ and the entropy of mixing simplifies to $\Delta_{mix}S = -n\,R\ln(2)$ such that the Gibbs free energy of mixing is

$$\Delta_{mix}G =\ -n\,R\,T\ln(2) \qquad \text{Eq. S6}$$

Equation S6 gives an estimate of the Gibbs free energy change associated with the transition from pure droplets of two different oils to equimolar mixed oil droplets. The Gibbs free energy of this exchange divided by a typical timescale over which the exchange occurs, Δt, gives the power production available to move the droplet pair. Assuming that the slowest step in the oil exchange process is transport into the aqueous phase, we estimate the oil exchange time from the measured solubilization rates of individual droplets, given in **Figure 3B**. We estimate that the oil exchange time is the time in which the volume of one droplet can be replaced entirely due to the combined transport rates of both droplets: $\Delta t \approx V_0\left(\frac{dV_1}{dt} + \frac{dV_2}{dt}\right)^{-1}$, where V_0 is the droplet's initial volume and $\frac{dV_1}{dt}$ and $\frac{dV_2}{dt}$ are the measured solubilization rates of both droplets. The average power produced by oil mixing (P_{in}) is the Gibbs free energy change of mixing divided by the mixing time, $P_{in} = \Delta_{mix}G/\Delta t$. Substituting for $\Delta_{mix}G$ using Eq. S6 and substituting for Δt, we find

$$P_{in} = -\frac{1}{V_0}\left(\frac{dV_1}{dt}n_1 + \frac{dV_2}{dt}n_2\right)R\,T\ln(2) \qquad \text{Eq. S7}$$

As an example, we measured that a pair consisting of one iodononane droplet and one iodopentane droplet with diameters of approximately 70 μm moves at 18 μm/s, so that the power required to move the pair is approximately $P_{out} = 1.9 \times 10^{-16}\ \mathrm{J/s}$. Individually, the

iodononane and iodopentane droplets solubilize at rates of $\frac{da}{dt} = 3.05\ \mathrm{nm/s}$ and $\frac{da}{dt} = 3.85\ \mathrm{nm/s}$, respectively. We use fact that the droplet size does not change significantly over the timescale on which chasing occurs such that $\frac{dV}{dt} = 4\pi a^2 \frac{da}{dt}$, and find *n* for each iodoalkane individually by dividing the droplet volume over the molecular volume of the oil $v_m = \frac{M_w}{\rho}$ where M_w is the oil molecular weight and ρ the density. We estimate a power production $P_{in} = -1.2 \times 10^{-9}\ \mathrm{J/s}$ using Eq. S7. This value *a posteriori* validates our assumption to ignore interfacial contributions which cannot exceed the interfacial free energy of the droplet $G_{interfacial} \approx A\,\gamma \approx 6 * 10^{-11}\,J$, estimated for the surface of a 70 µm droplet, $A = 1.5 * 10^{-8}\,m$, and an interfacial tension of iodoalkane oils in aqueous 0.5 wt% Triton X solution never exceeding $\gamma \approx 4 * 10^{-3} N/m$ as determined by pendant drop measurements.

Comparing P_{out} and P_{in} we find an efficiency $\epsilon = 1.6 \times 10^{-7}$. In conclusion, we find that the lower boundary of the swimming efficiency of the pairs of droplets described in this report is on the order of 10^{-7} which is two orders of magnitude higher than the typical efficiencies of 10^{-9} found for colloidal Janus swimmers whose motion is driven by the decomposition of hydrogen peroxide(*25*).

Microscopic mechanism behind droplet motion. There are two known microscopic mechanisms through which fluid particles can move in a solute concentration gradient, both driven by the molecular interactions between the solute and the surface of the particle (*14*). One mechanism relates to the chemophoretic contribution which involves a slip layer near the surface and a corresponding velocity difference between the surface of the particle and the fluid near the surface. This is the only contribution that matters for concentration-driven motion of solid particles, because a solid surface cannot flow. The surface of fluid particles, on the other hand, *can* flow, such that a gradient in solute concentration resulting in surface tension variation along the droplet surface can also drive motion of the particle by causing the fluid interface to move – i.e., the Marangoni effect. This mechanism does not have a fluid velocity jump across the interface but rather a stress jump, the Marangoni stress.

This distinction suggests that one could experimentally determine whether a given fluid particle's motion is caused by Marangoni or chemophoretic effects by measuring the fluid flow inside and outside the droplet. In practice, however, one would need to measure the flow velocity at distances to the interface comparable to the slip layer thickness, which is very challenging; this slip layer is on the order of the length scale of the microscopic interactions between the solute and the surface, which is typically in the 1-10 nm range. This length scale is smaller than the size of most tracer particles used to measure the flow and beyond the optical resolution used for imaging such that this is not a feasible experimental strategy. However, we can theoretically estimate which effect is likely to dominate using order of magnitude estimates of both contributions that have been comprehensively described in (*14*) and summarized in a very intuitive way in (*15*). The overall speed of the droplet v given by these two contributions is $v = -M' \nabla C$ with

$$M' \approx \frac{\pm k_B T a \lambda \pm k_B T \lambda^2 \frac{3\eta_i}{2\eta_0}}{2\eta_0 + 3\eta_i}, \qquad \text{Eq. S8}$$

where k_B is the Boltzmann constant, T the temperature a the particle radius, λ the lengthscale of

the interaction between the solute and the particle surface, η_i the viscosity of the fluid in the particle and η_0 the viscosity of the fluid outside the particle. The first term in this equation represents the Marangoni contribution and the second term represents the chemophoretic contribution. From this equation, one can identify (as Anderson and Izri et al. did) that the Marangoni contribution dominates when $\frac{a}{\lambda} \gg \frac{\eta_i}{\eta_0}$, whereas the chemophoretic effect dominates when $\frac{a}{\lambda} \ll \frac{\eta_i}{\eta_0}$. Typically, the length scale of interactions of the solute is on the order of the length scale of the solute, so on the order of 1 – 10 nm. So, for droplets on the length scale of several microns, the chemophoretic effect would only play a significant role when the viscosity of the droplet is 10^3 times higher than that of the continuous phase. For our specific case, $\lambda \approx 10$ nm, $a > 10$ µm, $\eta_i \approx \eta_o \approx 1\ \mathrm{mPa \cdot s}$, so that the contribution of the Marangoni effect dominates by more than a thousand-fold. We therefore conclude that the microscopic mechanism for the chasing motion of the droplets described in our experiments is the Marangoni effect.

Finally, we estimate the magnitude of the surface tension difference between the front and the back of the droplet that would lead to the typical speeds of 20 µm/s assuming that the Marangoni effect is the dominant responsible mechanism. We then compare this interfacial tension difference to the overall interfacial tension of the droplets as a sanity check. The speed of a droplet due to the Marangoni effect is (*40*):

$$v = M\nabla \mathrm{c} \text{ with } M = \frac{a}{2\eta_0 + 3\eta_i}\frac{d\gamma}{dc}. \qquad \text{Eq. S9}$$

Here M is the droplet's mobility, c the solute concentration, and γ the interfacial tension. Assuming a linear concentration gradient ($\nabla \mathrm{c} = \frac{dc}{dr}$) we can rewrite Equation S9 to find the interfacial tension gradient across the droplet as a function of its speed:

$$\frac{d\gamma}{dr} = \frac{v(2\eta_0 + 3\eta_i)}{a} \qquad \text{Eq. S10}$$

Using a typical speed of 20 µm/s, a droplet radius of 35 µm, and $\eta_0, \eta_i \approx 1$, we find that $\frac{d\gamma}{dr} \approx 2.9\ \mathrm{mN/m^2}$ so that the difference in surface tension between the front and the back of the droplet is approximately $\Delta\gamma \approx \frac{d\gamma}{dr} 2a \approx 0.2 * 10^{-3}\ \mathrm{mN/m}$. This is small compared to the typical interfacial tensions of iodoalkane oils in aqueous 0.5 wt% Triton solution which fall in the range of 1 to 4 mN/m as measured by pendant drop tensiometry, rendering the Marangoni effect a plausible mechanism for the observed droplet motion.